JACS
JOURNAL OF THE AMERICAN CHEMICAL SOCIETY
Article
pubs.acs.org/JACS

Anisotropic Chemical Pressure Effects in Single-Component Molecular Metals Based on Radical Dithiolene and Diselenolene Gold Complexes

Gilles Yzambart,[†] Nathalie Bellec,[†] Ghassan Nasser,[†] Olivier Jeannin,[†] Thierry Roisnel,[†] Marc Fourmigué,*[,†] Pascale Auban-Senzier,[‡] Jorge Íñiguez,[§] Enric Canadell,*[,§] and Dominique Lorcy*[,†]

[†]Institut des Sciences Chimiques de Rennes, UMR 6226 CNRS-Université de Rennes 1, Matière Condensée et Systèmes Electroactifs (MaCSE), Campus de Beaulieu, Bât 10A, 35042 Rennes cedex, France

[‡]Laboratoire de Physique des Solides, UMR 8502 CNRS-Université de Paris-Sud, Bat 510, F-91405 Orsay cedex, France

[§]Institut de Ciència de Materials de Barcelona (ICMAB-CSIC), Campus de la UAB, E-08193 Bellaterra, Spain

Supporting Information

ABSTRACT: On the basis of the reported radical neutral complex [Au(Et-thiazdt)$_2$] (Et-thiazdt = *N*-ethyl-1,3-thiazoline-2-thione-4,5-dithiolate), a series of single-component conductors derived from [Au(Et-thiazdt)$_2$], also noted as [AuS$_4$(=S)$_2$], has been developed, by replacing the outer sulfur atoms of the thiazoline-2-thione rings by oxygen atoms and/or by replacing the coordinating sulfur atoms by selenium atoms toward the corresponding diselenolene complexes. Comparison of the X-ray crystal structures and transport properties of the four isostructural complexes, noted as [AuS$_4$(=S)$_2$], [AuS$_4$(=O)$_2$], [AuSe$_4$(=S)$_2$], and [AuSe$_4$(=O)$_2$], shows that the oxygen substitution on the outer thiazoline ring actually decreases the conductivity by a factor of 100, despite a contracted unit cell volume reflecting a positive chemical pressure effect. On the other hand, the S/Se substitution increases the conductivity by a factor of 100, and the pressure needed to transform these semiconductors into the metallic state is shifted from 13 kbar in [AuS$_4$(=S)$_2$] to only ≈6 kbar in [AuSe$_4$(=S)$_2$]. Analysis of unit cell evolutions and ab initio band structure calculations demonstrates the strongly anisotropic nature of this chemical pressure effect and provides an explanation for the observed changes in conductivity. The greater sensitivity of these neutral single-component conductors to external pressure, as compared with "classical" radical salts, is also highlighted.

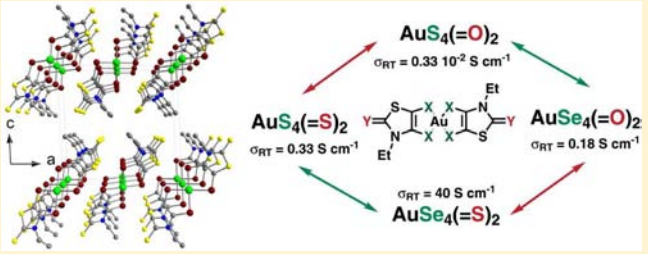

INTRODUCTION

Beyond the well-developed use of metal bis(dithiolene) complexes as precursors of multicomponent molecular conductors in mixed-valence salts such as C[Ni(dmit)$_2$]$_2$ (C$^+$ = NMe$_4^+$, TTF$^+$, ...),[1] an emerging strategy is to use these complexes as precursors of single-component molecular conductors, that is, *neutral* complexes lacking any C$^+$ counterion.[2] Along these lines, several neutral metal bis(dithiolene) complexes bearing a noninnocent tetrathiafulvalene backbone were successfully developed by Kobayashi et al., such as [Ni(tmdt)$_2$] (Chart 1).[3] Another route toward neutral single-component dithiolene complexes is based on neutral gold complexes lacking this TTF backbone.[4] Such radical species can be easily obtained by oxidation of the Au^{III} monoanionic dithiolene complexes, particularly with electron rich ligands like [Au(bdt)$_2$],[5] [Au(α-tpdt)$_2$],[6] and [Au(F$_2$pdt)$_2$][7] (Chart 1). The regular stacking of these radical complexes in the solid state[5,7] and the presence of interstack interactions allow for high room temperature conductivity (10^{-1}–10^{-3} S cm^{-1}), although the temperature dependence is characteristic of semiconducting behavior.

Chart 1

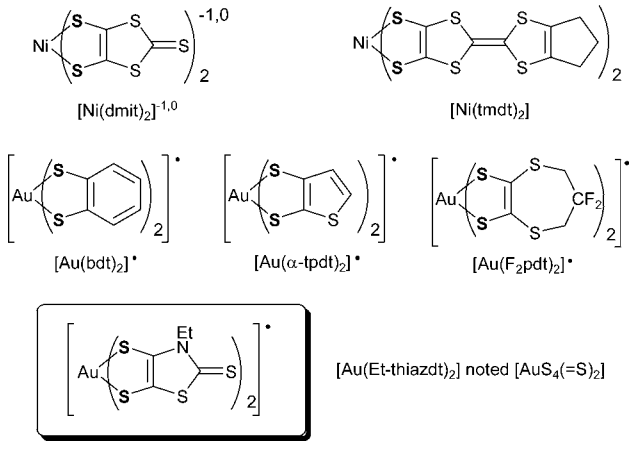

Received: July 10, 2012
Published: September 25, 2012

   dx.doi.org/10.1021/ja3065649 | J. Am. Chem. Soc. 2012, 134, 17138–17148

In this context, we recently reported the synthesis and properties of a very promising system based on the dithiolene ligand *N*-alkyl-1,3-thiazoline-2-thione-4,5-dithiolate (R-thiazdt).[8] Indeed, electrochemical oxidation of the anionic $[Au(Et\text{-}thiazdt)_2]^-$ afforded the neutral radical complex $[Au(Et\text{-}thiazdt)_2]$.[9] In the solid state, the radical complex organizes into uniform, nondimerized stacks, with sizable interstack interactions. Its room temperature conductivity is strongly pressure dependent, from 0.33 S cm^{-1} at ambient pressure up to 1000 S cm^{-1} at 21 kbar. Furthermore, from the room temperature semiconducting behavior, a metallic state can be stabilized above 13 kbar. Ab initio band structure calculations demonstrated unambiguously that the indirect gap observed at ambient pressure could be indeed suppressed by contracting the conducting slabs along the *b* stacking direction and/or the *a* interstack direction. Such theoretical approaches to pressure effects are particularly useful, as experimental structural determinations under pressure are still not a routine work.[10]

Because of the soft nature of molecular conductors, pressure has always been a favorite tool in the toolbox of solid-state physicists to explore the phase diagram of mixed valence multicomponent conducting salts, from hydrostatic[11] to uniaxial pressure effects.[12] *Chemical* substitution strategies offer another possibility to explore their phase diagram, as illustrated in the use of counterions of different volume in TMTTF[13,14] or TMTSF salts, for example, in the $PF_6^-/AsF_6^-/SbF_6^-$ or ClO_4^-/ReO_4^- series.[15,16] One can also mention the halide-containing salts such as κ-$[BEDT\text{-}TTF]_2[Cu(N(CN)_2)X]$[17] or $(o\text{-}Me_2TTF)_2X$,[18] with X = Cl, Br, I, or the (EDT-TTF-$CONMe_2$)X salts with X = Br or AsF_6.[19] Note also ternary compounds where the crystal structure includes solvent molecules of different size.[20] The effects of such substitutions have been described as *chemical pressure* effects. Positive chemical pressure effects are associated with smaller atoms or molecules, leading to a cell contraction with electronic consequences similar to those of an applied hydrostatic pressure, and negative pressure effects are associated with the more counterintuitive situation where larger unit cells lead to electronic behaviors observed only under higher pressures.[21] Deuteration has been also investigated in cation radical salts for that purpose as the volume of the CD_3 group has been estimated to be 1.0−1.5% less than that of the CH_3 group in the region of 50−100 K,[22] with different effects on metal−insulator or metal−superconductor transitions in TMTSF,[23] BEDT-TTF,[24] or DCNQI salts.[22]

Single-component conductors such as $[Au(tmdt)_2]$[25] are also pressure sensitive,[26] as well as organic radicals[27] behaving as Mott insulators,[28] which exhibit an insulator to metal transition under high pressure.[29] The striking physical pressure effects unraveled in the single-component $[Au(Et\text{-}thiazdt)_2]$ conductor[9] raise questions about the possible effects that *chemical pressure* could play within these single-component conductors. In the absence of any counterion, the only possibility left for investigating chemical pressure effects is based on atom substitution on the thiazdt backbone of the organic ligand. We have thus followed two different strategies to test the chemical pressure influence. In the one hand, we focused our attention on the exocyclic sulfur atoms of the reference complex $[Au(Et\text{-}thiazdt)_2]$, noted as $[AuS_4(=S)_2]$ in the following to highlight the modified atoms on the Et-thiazdt ligand. Indeed, these two exocyclic sulfur atoms do not participate notably in the interactions between neighboring molecules in the conducting slabs. It was therefore anticipated that the introduction of smaller oxygen atoms could bring the molecules closer to each other and exert a positive chemical pressure on the system. Accordingly, we have prepared the *N*-ethyl-1,3-thiazoline-2-one-4,5-dithiolate ligand and its corresponding neutral gold bis(dithiolene) complex, noted as $[AuS_4(=O)_2]$. On the other hand, we also investigated the introduction of heavier selenium atoms in the metallacycles, as the S/Se substitution usually increases intermolecular interactions and consequently band dispersion in the solid state. Accordingly, we have prepared the two novel diselenolate ligands, i.e., *N*-ethyl-1,3-thiazoline-2-one-4,5-diselenolate and *N*-ethyl-1,3-thiazoline-2-thione-4,5-diselenolate and their corresponding Au bis(diselenolene) complexes, noted as $[AuSe_4(=O)_2]$ and $[AuSe_4(=S)_2]$, respectively (Chart 2).

Chart 2

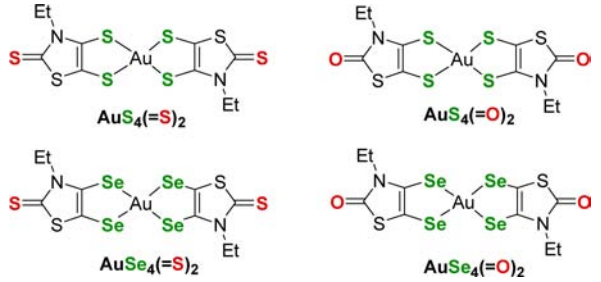

In this paper, we describe the structural and electronic properties of the monoanionic species based on the three analogues of the all-sulfur $[AuS_4(=S)_2]^{-1}$ complex, that is, $[AuS_4(=O)_2]^{-1}$, $[AuSe_4(=O)_2]^{-1}$, and the $[AuSe_4(=S)_2]^{-1}$, and their oxidation to the corresponding neutral radical complexes. The observed striking evolutions of their transport properties within the whole series are rationalized on the basis of a combined experimental and theoretical approach to their crystallographic and electronic structures, demonstrating that atom substitutions can afford highly *anisotropic* chemical pressure effects, an original approach besides uniaxial physical pressure effects to explore the phase diagram of these single-component molecular conductors.

RESULTS AND DISCUSSION

Synthesis and Crystal Structures. The synthesis of the monoanionic gold dithiolene and diselenolene complexes was carried out starting from the *N*-ethyl-1,3-thiazoline 2-thione **1**, according to the synthetic strategy described in Scheme 1. In

Scheme 1. Synthetic Procedures toward Anionic Gold Complexes

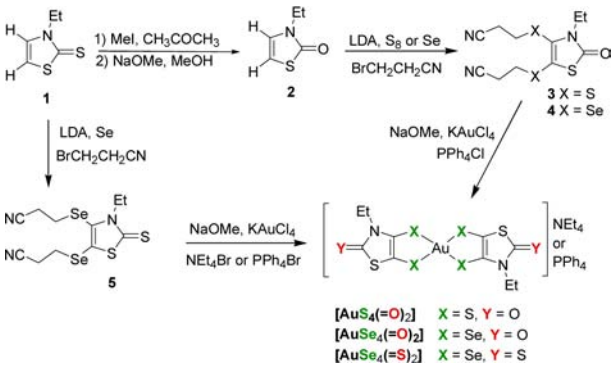

dx.doi.org/10.1021/ja3065649 | J. Am. Chem. Soc. 2012, 134, 17138−17148

order to form the *N*-ethyl-1,3-thiazoline-2-one **2**, we first transformed **1** into the corresponding thiomethyl-1,3-thiazolium salt, thanks to the alkylation of the exocyclic sulfur atom with MeI. The subsequent reaction of this salt with MeONa allowed us to isolate **2** in 82% yields. Then, we synthesized the organic hidden form of the dithiolate and diselenolate ligands, where these ligands are protected by cyanoethyl groups. The protected dithiolate and diselenolate ligands were formed by reacting the thiazole rings **1** and **2** at −10 °C in THF with successively (i) lithium diisopropylamide (LDA), (ii) sulfur or selenium, and (iii) 3-bromopropionitrile (Scheme 1). These organic hidden forms of the ligands are easily purified by column chromatography. Deprotection of the dithiolate and diselenolate ligands was realized in basic medium using sodium methanolate. Then $KAuCl_4$ was added to the solution, followed by the addition of Et_4NBr or PPh_4Cl to the reaction mixture. The corresponding dithiolene complexes $[PPh_4][AuS_4(=O)_2]$ and the diselenolene monoanionic gold complexes $[PPh_4][AuSe_4(=O)_2]$ and $[NEt_4][AuSe_4(=S)_2]$ were isolated in 30−50% yields. Black crystals, suitable for X-ray diffraction studies were obtained for every complex after recrystallization in acetonitrile.

The molecular structures of the anionic moieties of the three complexes depicted in Figure 1 show the same trends: (i) a

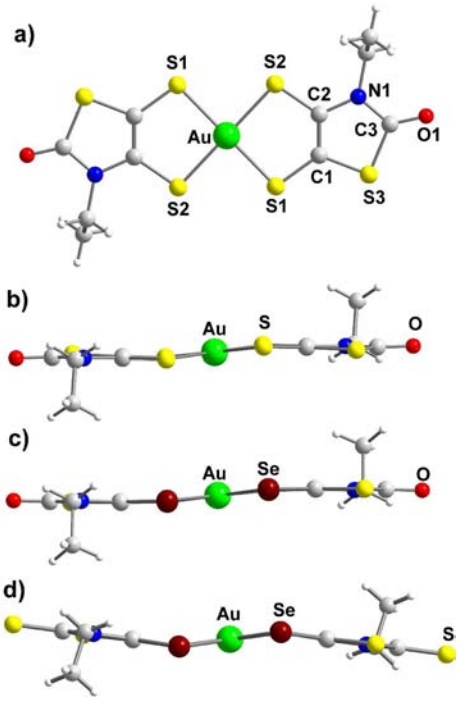

Figure 1. Molecular structure of the monoanionic species in $[PPh_4][AuS_4(=O)_2]$ (a) and side views of the monoanionic species in $[PPh_4][AuS_4(=O)_2]$ (b), $[PPh_4][AuSe_4(=O)_2]$ (c), and $[NEt_4][AuSe_4(=S)_2]$ (d).

square-planar geometry around the Au atom, (ii) the obtention of the trans isomer only, even if the cis and trans isomers can be formed due to the dissymmetry of the dithiolene ligands, and (iii) the metallacycles are nonplanar and are folded along the X···X axis (X = S, Se) with an angle of about 5°−17° while the outer thiazole cores are planar. These geometrical features are similar to those observed on the analogous monoanionic gold dithiolene complex, $[NEt_4][AuS_4(=S)_2]$.[9] Intramolecular bond lengths (Table 1) within the metallacycles are comparable to

Table 1. Intramolecular Bond Lengths (in Å) in Monoanionic and Neutral Dithiolene and Diselenolene Complexes $[AuS_4(=S)_2]^{-,\bullet}$, $[AuS_4(=O)_2]^{-,\bullet}$, $[AuSe_4(=S)_2]^{-,\bullet}$, and $[AuSe_4(=O)_2]^{-,\bullet}$, Together with the Folding Angle of the Metallacycle along the Chalcogen···Chalcogen Axis, $\theta_{S\cdots S}$ and $\theta_{Se\cdots Se}$

	$[AuS_4(S)_2]^-$ [9]	$[AuS_4(S)_2]^\bullet$ [9]	$[AuS_4(O)_2]^-$	$[AuS_4(O)_2]^\bullet$
Au−S1	2.3321(16)	2.3196(13)	2.317(1)	2.309(3)
Au−S2	2.3287(15)	2.3186(14)	2.326(1)	2.322(3)
S1−C1	1.744(6)	1.713(5)	1.740(3)	1.708(12)
S2−C2	1.760(5)	1.720(6)	1.750(2)	1.738(11)
C1−C2	1.332(8)	1.372(8)	1.338(4)	1.379(17)
C2−N1	1.416(7)	1.390(7)	1.402(3)	1.389(14)
C1−S3	1.731(6)	1.738(5)	1.751(3)	1.736(12)
N1−C3	1.356(7)	1.370(7)	1.371(3)	1.370(15)
S3−C3	1.743(6)	1.749(6)	1.787(3)	1.799(13)
C3−X4	1.658(6)	1.641(6)	1.215(3)	1.206(15)
$\theta_{S\cdots S}$	10.9(1)	1.2(1)	8.42(5)	0.6(2)
	$[AuSe_4(O)_2]^-$	$[AuSe_4(O)_2]^\bullet$	$[AuSe_4(S)_2]^-$	$[AuSe_4(S)_2]^\bullet$
Au−S1	2.433(2)	2.4432(17)	2.4405(6)	2.4368(3)
Au−S2	2.445(2)	2.4164(17)	2.4456(6)	2.4410(4)
Se1−C1	1.879(7)	1.833(17)	1.874(6)	1.862(4)
Se2−C2	1.902(6)	1.903(18)	1.910(6)	1.875(4)
C1−C2	1.339(10)	1.42(3)	1.342(8)	1.374(5)
C2−N1	1.395(8)	1.38(2)	1.398(7)	1.390(4)
C1−S3	1.761(7)	1.729(17)	1.739(6)	1.740(3)
N1−C3	1.36(1)	1.36(2)	1.369(7)	1.373(5)
S3−C3	1.792(8)	1.83(2)	1.749(6)	1.755(4)
C3−X4	1.218(10)	1.18(2)	1.659(6)	1.649(4)
$\theta_{Se\cdots Se}$	5.7(2)	0.4(4)	16.8(1)	2.82(5)

those observed for other monoanionic homoleptic gold dithiolene or diselenolene complexes, with Au−Se bond distances around 2.44 Å and Au−S bond distances around 2.32 Å. The main difference induced by the outer chalcogen atom is observed in the folding angle along the X···X axis, which is significantly smaller in the thiazoline-2-one when compared with the thiazoline-2-thione. This can be ascribed to the difference of electronegativity/polarizability of the outer chalcogene atom.

Electrochemical Studies. Cyclic voltammograms (CV) of the three novel anionic complexes have been recorded in CH_2Cl_2 using $[NBu_4][PF_6]$ as supporting electrolyte. The CV of $[PPh_4][AuS_4(=O)_2]$ is shown in Figure 2 as an example. $[PPh_4][AuS_4(=O)_2]$ and $[PPh_4][AuSe_4(=O)_2]$ exhibit upon anodic investigation two reversible monoelectronic processes corresponding to the oxidation of the monoanionic species into the neutral radical and then to the oxidation into the monocationic species. Upon cathodic investigation, the reduction wave is irreversible and corresponds to the reduction

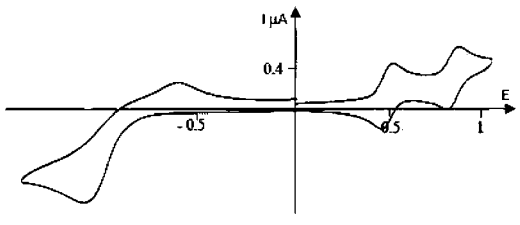

Figure 2. Cyclic voltammogram of $[PPh_4][AuS_4(=O)_2]$ in CH_2Cl_2 with 0.1 M $[NBu_4][PF_6]$ as electrolyte (*E* in V vs SCE, scan rate 100 mV s^{-1}).

dx.doi.org/10.1021/ja3065649 | J. Am. Chem. Soc. 2012, 134, 17138−17148

into the dianionic species. As already observed for Ni complexes with similar ligands,[8a] the first oxidation process of the dithiolene $[AuS_4(=O)_2]^-$ occurs at a less anodic potential than for the corresponding diselenolene $[AuSe_4(=O)_2]^-$ (Table 2). Note also that the substitution of sulfur for oxygen

Table 2. Redox Potentials for the Various Gold Dithiolene and Diselenolene Complexes in CH_2Cl_2 with 0.1 M $[NBu_4][PF_6]$ (E in V vs SCE, ν = 100 mV s^{-1})

complex	E_{red}	E^1_{ox}	E^2_{ox}	ref
$[AuS_4(=O)_2]$	−1.05[a]	0.39	0.86	this work
$[AuSe_4(=O)_2]$	−1.07[a]	0.44	0.88	this work
$[AuSe_4(=S)_2]$	−0.89[a]	0.52[a]	–	this work
$[AuS_4(=S)_2]$	−0.90[a]	0.52	0.65	9

[a]Irreversible process.

increases the overall electron-donating ability of the complexes, as illustrated by the comparison of the first redox potential of $[AuS_4(=O)_2]^-$ (+0.38 V) with that of $[AuS_4(=S)_2]^-$ (+0.52 V). The diselenolene complex $[AuSe_4(=S)_2]^-$ shows a different behavior, as an irreversible oxidation process is observed at 0.52 V on the first anodic scan, presumably due to adsorption phenomena.

The Neutral Radical Complexes. Oxidation of the monoanionic species has been realized electrochemically upon application of a current intensity of 0.2−0.5 μA in the presence of NBu_4PF_6 as supporting electrolyte. Crystals of the neutral species were collected on the anode and investigated by X-ray diffraction. The neutral complexes $[AuS_4(=O)_2]$, $[AuSe_4(=O)_2]$, and $[AuSe_4(=S)_2]$ crystallize in the monoclinic system, space group $P2_1/a$. They are isostructural with the all-sulfur analog $[AuS_4(=S)_2]$.[9] The molecular structures of the three complexes show that all these neutral species are planar, as depicted in Figure 3 for $[AuSe_4(=O)_2]$, with a chalcogen···chalcogen folding angle ($\theta_{S\cdots S}$ and $\theta_{Se\cdots Se}$ in Table 1) strongly decreased, when compared with the monoanionic complexes.

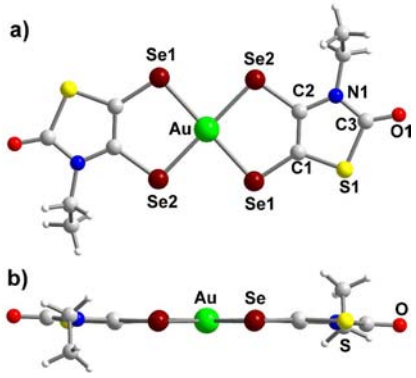

Figure 3. Molecular structure of the neutral species $[AuSe_4(=O)_2]$.

Comparison of the geometrical characteristics between the monoanionic and neutral states of the complexes allowed us to analyze the modifications occurring upon oxidation (Table 1). These modifications occur essentially on the bond lengths of the metallacycles and follow the same trends for the dithiolene and the diselenolene derivatives. For instance, upon oxidation, the X−C (X = S, Se) bonds are shortened while the C=C bond is lengthened. Apart from this C=C bond, the other bonds in the outer thiazole ring are not significantly modified. These structural modifications upon oxidation demonstrate the strong delocalization of the spin density on the metallacycles, as already observed with the few examples of gold dithiolene complexes reported so far where both monoanionic and neutral forms were characterized, that is, $[Au(\alpha\text{-tpdt})_2]$,[6] $[Au(dddt)_2]$,[30,31] $[Au(F_2pdt)_2]$,[7] and $[AuL_2]$ with L = 1,2-di(4-*tert*-butylphenyl)ethylene-1,2-dithiolate.[32] In the solid state (Figure 4), the neutral radical complexes adopt the same

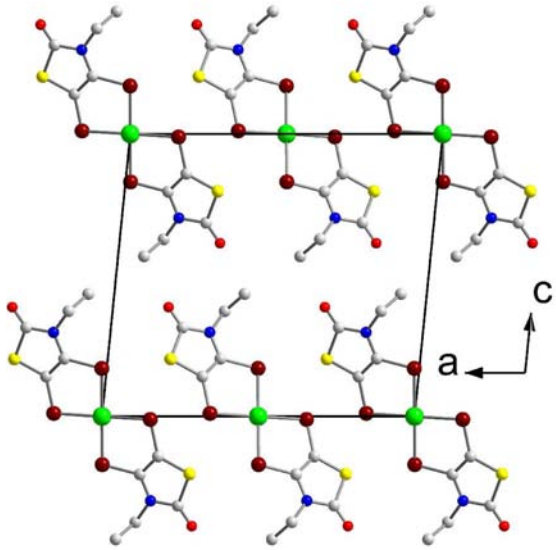

Figure 4. Projection view along b of the unit cell of $[AuSe_4(=O)_2]$.

structure as $[AuS_4(=S)_2]$, characterized by a layered structure, with uniform stacks running along b and interacting laterally along a. Within the stacks, a lateral slip is observed between neighboring complexes.

We have therefore now at hand a series of four isostructural radical complexes, with either S or O atoms on the outer thiazoline ring, with either S or Se atoms to coordinate the gold atom. The all-sulfur compound, $[AuS_4(=S)_2]$ was reported to behave as a semiconductor at ambient pressure, with σ_{RT} = 0.33 S cm^{-1} and E_{act} = 0.12 eV [$\rho = 1/\sigma = \rho_0 \exp(E_{act}/kT)$]. It becomes metallic at pressures above 13 kbar.[9]

The resistivity measurements (Figure 5) were carried out on single crystals of the three novel complexes along the long axis of the needles (b crystallographic axis). The room temperature

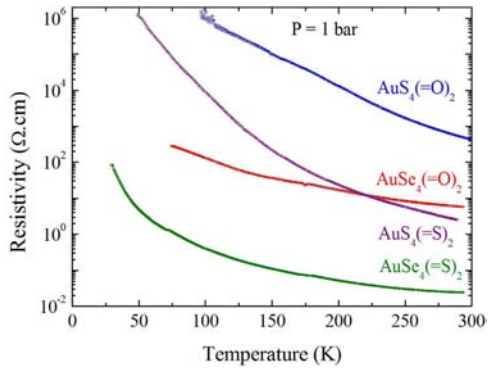

Figure 5. Temperature dependence of the resistivity of the four complexes at ambient pressure.

dx.doi.org/10.1021/ja3065649 | J. Am. Chem. Soc. 2012, 134, 17138−17148

conductivity at ambient pressure, σ_{RT} (1 bar), is 0.33×10^{-2} S cm^{-1} for [AuS$_4$(=O)$_2$], 0.18 S cm^{-1} for [AuSe$_4$(=O)$_2$], and 40 S cm^{-1} for [AuSe$_4$(=S)$_2$].

Upon cooling, a semiconducting behavior is observed for the three complexes with activation energies (determined between 200 and 300 K) of 0.18, 0.06, and 0.05 eV for [AuS$_4$(=O)$_2$], [AuSe$_4$(=O)$_2$], and [AuSe$_4$(=S)$_2$], respectively. It follows that the replacement of the outer sulfur atom by oxygen actually decreases σ_{RT} (1 bar) by 2 orders of magnitude, while the replacement of the coordinating sulfur atoms with selenium atoms increases σ_{RT} (1 bar) by 2 orders of magnitude. The two combined substitutions cancel each other in [AuSe$_4$(=O)$_2$] compared to the original [AuS$_4$(=S)$_2$], but the activation energy is smaller in the diselenolene compound. These trends are also confirmed by the temperature dependence of the paramagnetic susceptibility, determined for the three compounds in the 2−300 K temperature range (Figure 6). Two

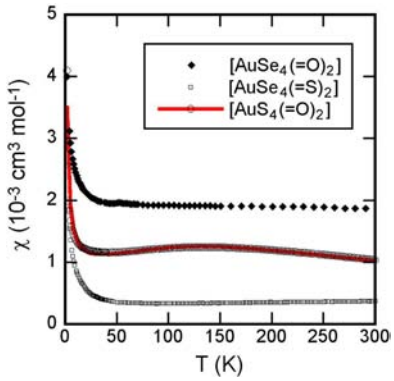

Figure 6. Temperature dependence of the paramagnetic susceptibility of [AuS$_4$(=O)$_2$], [AuSe$_4$(=O)$_2$], and [AuSe$_4$(=S)$_2$]. The red line is a fit to the Bonner−Fischer model (see text) for the less conducting [AuS$_4$(=O)$_2$] compound.

different behaviors can be observed. Indeed, for [AuS$_4$(=O)$_2$], the magnetic susceptibility is weakly temperature dependent (10^{-3} cm^3 mol^{-1}) and well fitted with a Bonner−Fisher model for a uniform spin chain with J/k = −211(4) K (J = −144 cm^{-1}), together with a Curie tail amounting to 1.4% magnetic defaults, indicating a stronger spin localization associated with a less conducting behavior. Contrariwise, the paramagnetic susceptibility for the more conducting [AuSe$_4$(=O)$_2$] and [AuSe$_4$(=S)$_2$] diselenolene compounds, corrected for the Pascal diamagnetic term, is almost temperature independent. The smaller value is observed with the most conducting [AuSe$_4$(=S)$_2$] compound. A Curie tail at the lowest temperatures corresponds to only 0.47 and 1.2% of $S = {}^1/_2$ species attributable to paramagnetic defaults in [AuSe$_4$(=O)$_2$] and [AuSe$_4$(=S)$_2$], respectively.

Anisotropic Chemical Pressure Effect. While the increase of conductivity and decrease of activation energy upon selenium substitution could be anticipated, the opposite behavior upon oxygen introduction appears very surprising, also considering that the unit cell volume does indeed decrease notably when replacing the exocyclic sulfur atoms by oxygen atoms. However, as shown in Figure 7, this unit cell contraction is far from isotropic. Indeed, the unit cell volume contraction is actually accompanied by a notable expansion along the *a* and *b* axes of the unit cell (in red in Figure 7), demonstrating that the anticipated positive chemical pressure effect is actually reversed

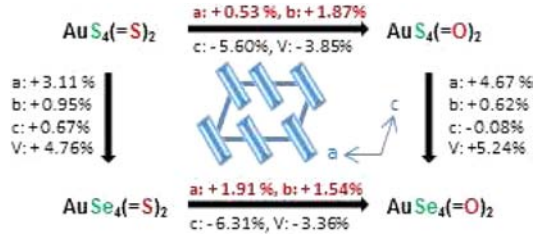

Figure 7. Evolution of the unit cell parameters within the series. The negative pressure effects are highlighted in red.

in the (*a*, *b*) conducting planes, with important consequences on the intermolecular interactions.

Indeed, as illustrated below in Figure 8 for the two selenolate complexes [AuSe$_4$(=S)$_2$] and [AuSe$_4$(=O)$_2$], the shortest

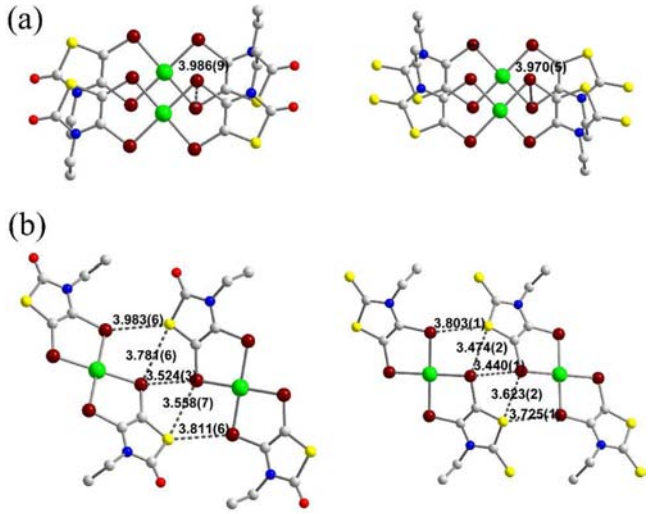

Figure 8. View of the short Se···Se and S···Se contacts between neighboring [AuSe$_4$(=O)$_2$] (left) and [AuSe$_4$(=S)$_2$] (right) (a) within the stacks and (b) between two neighboring stacks.

intrastack (Figure 8a) and interstack (Figure 8b) intermolecular S···S, Se···Se, or S···Se contacts are actually longer when we replace the outer sulfur atom in [AuSe$_4$(=S)$_2$] by an oxygen atom in [AuSe$_4$(=O)$_2$]. Similar trends are found when going from [AuS$_4$(=S)$_2$] to [AuS$_4$(=O)$_2$].

If we now concentrate on the influence of the nature of the chalcogen atom within the metallacycles, for example by comparing the unit cell dimensions of [AuS$_4$(=S)$_2$] and [AuSe$_4$(=S)$_2$], or [AuS$_4$(=O)$_2$] and [AuSe$_4$(=O)$_2$], we can observe that the effect of the S/Se substitution is also highly anisotropic (Figure 7), as it mainly affects the *a* axis associated with lateral interactions between stacks within the conducting slabs. Besides, the increase along the *b* stacking axis is considerably smaller than what would be expected from the difference of S and Se van der Waals radii (evolution of the van der Waals radii when going from one S atom to one Se is +5.26%). Therefore, stronger interactions are observed within the diselenolene series along both the *a* and *b* axes. These interactions are even more pronounced with the diselenolene bearing outer sulfur atoms, [AuSe$_4$(=S)$_2$].

These combined results corroborate the information obtained from transport and magnetic measurements. The presence of the smaller oxygen atoms in [AuS$_4$(=O)$_2$], when compared with the original all sulfur [AuS$_4$(=S)$_2$] complex,

dx.doi.org/10.1021/ja3065649 | J. Am. Chem. Soc. 2012, 134, 17138−17148

induces a compression along the *c* axis, making the slabs closer to each other but creating a concomitant dilatation along the *a* and *b* axes, within the conducting slabs. As a consequence, the conductivity of $[AuS_4(=O)_2]$ is 100 times lower than that of the all sulfur analog and the activation energy is higher. Concerning the diselonolate complex $[AuSe_4(=S)_2]$, a 100 times increase of the conductivity is observed as it reaches 40 S cm^{-1} at room temperature. Upon cooling, a semiconducting behavior is observed with much smaller activation energy than for the dithiolene analog. In the $[AuSe_4(=O)_2]$ complex, replacement of the sulfur atoms by selenium ones counterbalances the effect of the exocyclic oxygen atoms. Actually, the conductivity measured for $[AuSe_4(=O)_2]$ is approximately the same as the one determined for $[AuS_4(=S)_2]$ (Figure 5).

Physical Pressure Effects, Compressibility, and Modelization. The evolution of the conductivity of $[AuS_4(=S)_2]$ under pressure has been already reported.[9] The all-sulfur complex becomes metallic above 13 kbar, and the metal–insulator transition that appeared below 70 K is totally suppressed above 17 kbar. It is therefore interesting at this stage to compare this behavior with that of the most conducting member of the series, that is, $[AuSe_4(=S)_2]$.

As mentioned above, $[AuSe_4(=S)_2]$ shows an 100-fold increase in conductivity at ambient temperature and pressure. Under pressure, its room temperature conductivity increases strongly, from 40 to 2600 S cm^{-1} at 12.5 kbar, and exhibits two different regimes (Figure 9). An exponential pressure dependence is first observed up to 4 kbar followed by a linear pressure dependence above 6 kbar. These two different regimes can be associated with a semiconducting behavior below 4 kbar (with a linear variation of the activation energy with pressure) and a metallic behavior above 6 kbar. The same feature was already observed for $[AuS_4(=S)_2]$ but with a regime change at higher pressure (around 13 kbar),[9] i.e., shifted by 9 kbar.

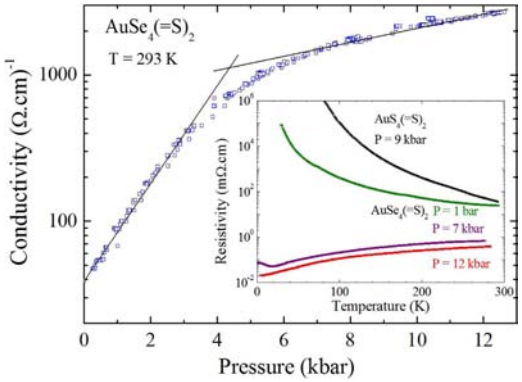

Figure 9. Pressure dependence of the room temperature conductivity of $[AuSe_4(=S)_2]$. The black lines are guides to the eye. Inset: temperature dependence of the resistivity of $[AuSe_4(=S)_2]$ at ambient pressure (green), 7 kbar (purple), and 12 kbar (red) and for comparison $[AuS_4(=S)_2]$ at 9 kbar (black).

This 9 kbar shift also appears when comparing the temperature dependence of the resistivity for $[AuSe_4(=S)_2]$ at ambient pressure (insert of Figure 9) with the data obtained for $[AuS_4(=S)_2]$ under different pressures.[9] We note a similarity between the behavior of $[AuSe_4(=S)_2]$ at ambient pressure and $[AuS_4(=S)_2]$ at 9 kbar (also plotted in the inset of Figure 9), with an even smaller activation energy. However, the comparison between activation energies determined at different applied pressures on different compounds is not quite reliable because of the volume changes during cooling. Finally, the change of regime for the conductivity observed above 6 kbar is confirmed by the metallic temperature dependencies of the resistivity for $[AuSe_4(=S)_2]$ at 7 and 12 kbar (inset of Figure 9).

The 9 kbar chemical pressure value associated with the S_4/Se_4 substitution can be compared with similar pressure effects reported in an isostructural series of organic conductors such as the TMTTF–TMTSF salts. In the generic phase diagram of these salts, Jérome reported indeed a 26 kbar shift between the sulfur salt, $(TMTTF)_2PF_6$, and the selenium salt, $(TMTSF)_2PF_6$.[33] The much smaller 9 kbar chemical pressure effect observed here tends to indicate a higher sensitivity of the neutral single component structures investigated here, by contrast with ionic multicomponent radical salts.

In our previous paper on the all sulfur complex $[AuS_4(=S)_2]$, first principles band structure calculations have shown the presence of a small indirect gap, while simulations for slightly compressed cells along the *a* (transverse) and *b* (stacking) directions were able to show that the gap closes and the metallic state is stabilized. Analogous calculations were performed here for the whole series. Using the experimental crystal structures, we have found that the delocalized (metallic) and localized (antiferromagnetic, AFM) states differ by a small energy difference and compete for the ground state in all these solids. The localized AFM state is the ground state for $[AuS_4(=S)_2]$, $[AuS_4(=O)_2]$, and$[AuSe_4(=O)_2]$, whereas the metallic state is favored for $[AuSe_4(=S)_2]$. The AFM state is made of stacks with molecules with an unpaired spin up and down alternating along *b*. The calculated band structures for the ground state of the four systems are reported in Figure 10 (in those for the AFM systems every band is the superposition of two bands, one associated with spin up and localized in one of every two molecules along the stacks and the other with spin down is localized in the other set of molecules along the stack, whereas in that of the metallic systems both bands are equally delocalized). As noted for other gold bis(dithiolene) complexes,[7] the singly occupied molecular orbital (SOMO) and the orbital immediately below (SOMO−1) differ by an energy that is on the same order of magnitude as the intermolecular transfer integrals. This leads to the overlap of the SOMO and SOMO−1 bands with the consequence that, in contrast with most molecular conductors, two bands per molecule must be explicitly considered. Although the crystallographic unit cell contains only two molecules, we had to double it in order to be able to describe the antiferromagnetic state. Consequently, the band structures of Figure 10 contain eight bands, four originating from the SOMO and four from the SOMO−1. Since every molecule contributes with three electrons to the bands, six pairs of bands should be filled. Note the small indirect gap separating the sixth and seventh pairs of bands in the band structures of the $[AuS_4(=S)_2]$ and $[AuSe_4(=O)_2]$ (Figure 10, parts b and c, respectively) and the noticeably larger gap in that of $[AuS_4(=O)_2]$ (Figure 10d). Two pairs of bands overlap at the Fermi level in the band structure of $[AuSe_4(=S)_2]$ (Figure 10a) which thus corresponds to a metallic state. Thus, taking into account the usual overestimation of the stability of the metallic state in DFT, the band structures of Figure 10 suggest that $[AuS_4(=S)_2]$ and $[AuSe_4(=O)_2]$ should have similar conductivities, whereas $[AuS_4(=O)_2]$ and $[AuSe_4(=S)_2]$ should exhibit lower and higher conductivities, respectively, in nice agreement with the above experimental

dx.doi.org/10.1021/ja3065649 | J. Am. Chem. Soc. 2012, 134, 17138–17148

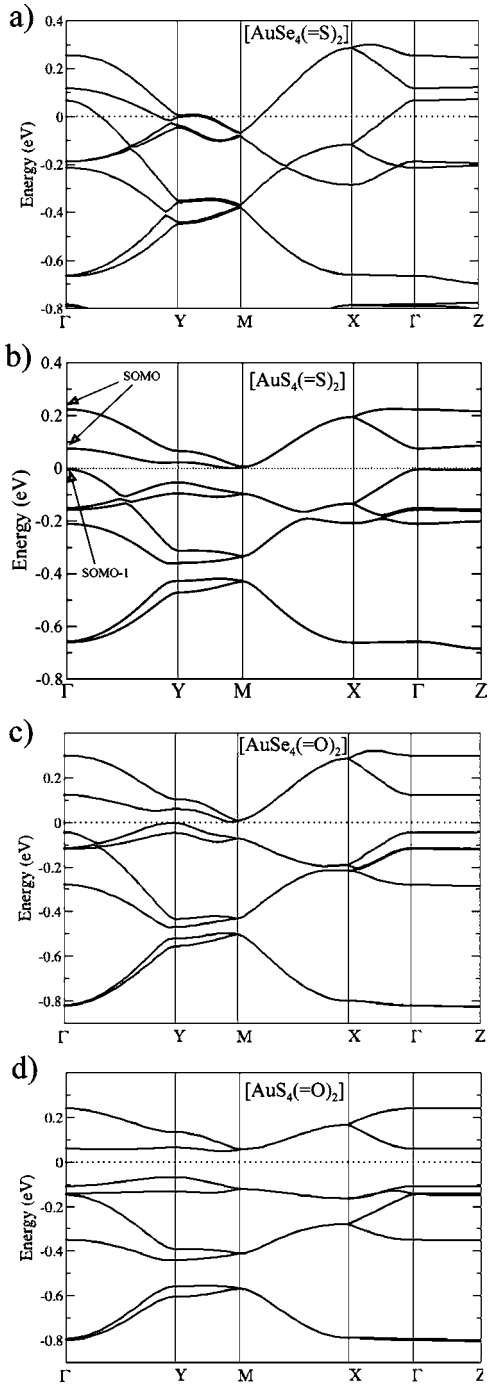

Figure 10. Band structure for the metallic ground state of $[AuSe_4(=S)_2]$ (a) and the antiferromagnetic ground state of $[AuS_4(=S)_2]$ (b), $[AuSe_4(=O)_2]$ (c), and $[AuS_4(=O)_2]$ (d). The dotted line refers to the Fermi level in part a and the highest occupied level of the system in parts b–d. Γ, X, Y, Z, and M refer to the (0, 0, 0), ($^1/_2$, 0, 0), (0, $^1/_2$, 0), (0, 0, $^1/_2$), and ($^1/_2$, $^1/_2$, 0) points of the monoclinic Brillouin zone.

results. Except for $[AuS_4(=O)_2]$, there is a very small indirect band gap around the Fermi level (and this must also apply for $[AuSe_4(=S)_2]$ because of the above-mentioned overstabilization of the metallic state in DFT), and consequently, the conduction should be activated. However, because of the very weak gap the materials may be considered in practice as semimetals, thus explaining the fact that whereas the conductivity is activated (although with a small activation energy), the magnetic susceptibility shows a Pauli-type paramagnetic behavior, typical of metallic systems.

The nature of the different bands was previously discussed in detail for $[AuS_4(=S)_2]$.[9] In the context of the present work, it is important to emphasize that, as noted in Figure 10b, the top two bands at Γ originate from the SOMO and the third band from the top originates from the SOMO−1. The width of the SOMO and SOMO−1 bands strongly depend on the strength of the interactions along the stack direction (i.e., the *b*-direction). The SOMO and SOMO−1 are very directional π-type orbitals making strong interactions along the stacks. Thus, since replacement of Se for S in the central backbone of the molecules leads to a reinforcement of these interactions, the indirect gap decreases (and eventually disappears), leading to an increase in the conductivity.

To analyze the effect of the replacement of O for S in the outer part of the molecule, it is interesting to run simulations for slightly expanded cells along the *a*- and *b*-directions. As it is clear from Figure 10, the conductivity of these materials increases with the width of the upper SOMO and SOMO−1 bands, which leads to the decrease of the indirect band gap and eventually to the semimetallic overlap. In the simulations that we have carried out, the molecules were moved rigidly along the chosen directions. The calculated band structures when the molecules move away by 0.2 Å are shown in Figure 11. Note that the band structure for $[AuSe_4(=S)_2]$ with expansion along both the *a*- and *b*-directions (Figure 11c) is almost identical to that of $[AuS_4(=S)_2]$ (Figure 10b). It turns out that the band structure is especially sensitive to the expansion along the stacking *b*-direction. Since as examined above the volume decrease resulting from the O for S replacement is associated with an increase in the *a* and *b* cell constants (Figure 7), the simulations of Figure 11 provide a simple rationale for the observed conductivity decrease.

■ CONCLUSIONS

Chemical pressure effects by atom substitution are known to play an important role in molecular conductors. We have shown here within an original series of single-component conductors derived from $[Au(Et\text{-}thiazdt)_2]$ that such effects are actually strongly anisotropic. The replacement of sulfur by oxygen atoms when going from $[AuS_4(=S)_2]$ to $[AuS_4(=O)_2]$ induces indeed a reduced cell volume but a concomitant dilatation of the conducting slabs with an associated 100-fold reduced conductivity. Similar trends are found in the diselenolene series. Such effects should be carefully considered in the future when discussing positive or negative chemical pressure effects. Of particular note is also the high sensitivity of such neutral single-component conductors—by comparison with multicomponent salts—to external pressure, a sensitivity attributable to their neutral, more compressible character. Analysis of unit cell evolutions and ab initio band structure calculations demonstrate the strongly anisotropic nature of this chemical pressure effect and provide an explanation for the observed changes in conductivity.

■ EXPERIMENTAL SECTION

General. All commercial reagents were used as purchased. The thiazoline-2-thione **1** was synthesized according to a literature procedure.[9] All air-sensitive reactions were carried out under an argon atmosphere. Melting points were measured on a Kofler hot-stage apparatus and are uncorrected. ^{1}H NMR and ^{13}C NMR spectra were recorded on a Bruker AV300III spectrometer. Chemical shifts are

dx.doi.org/10.1021/ja3065649 | J. Am. Chem. Soc. 2012, 134, 17138–17148

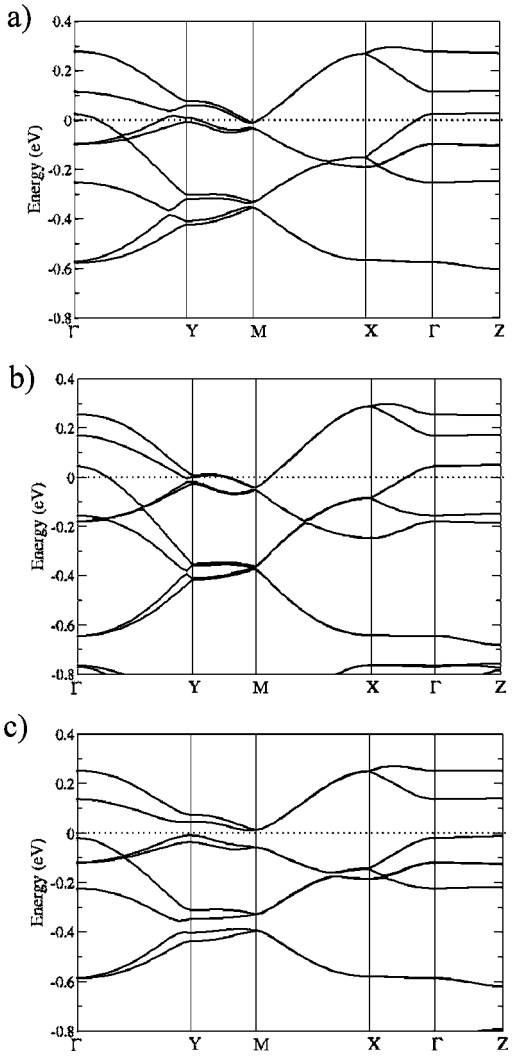

Figure 11. Band structure calculated for $[AuSe_4(=S)_2]$ when the molecules are rigidly separated by 0.2 Å along (a) the stacking *b*-direction, (b) the interstack *a*-direction, and (c) along both the stacking *b*- and interstack *a*-directions. The dotted line refers to the Fermi level in parts a and b, and the highest occupied level of the system in part c.

quoted in parts per million (ppm) referenced to tetramethylsilane. Mass spectra were recorded with Varian MAT 311 instrument by the Centre Régional de Mesures Physiques de l'Ouest, Rennes, France. Elemental analyses were performed at the Centre Régional de Mesures Physiques de l'Ouest, Rennes, France. Tetrahydrofuran was distilled from sodium−benzophenone. Column chromatography was performed using silica gel Merck 60 (70−260 mesh). Cyclic voltammetry was carried out on a 10^{-3} M solution of the complex in CH_3CN or in CH_2Cl_2, containing 0.1 M *n*-Bu_4NPF_6 as supporting electrolyte. Voltammograms were recorded at 0.1 V s^{-1} on a platinum disk electrode (A = 1 mm^2). The potentials were measured versus a saturated calomel electrode (SCE).

1,3-Thiazoline-2-one 2. To a solution of 1,3-thiazoline-2-thione **1** (4 g, 27.6 mmol) in dry acetone (30 mL) was slowly added iodomethane (2.1 mL, 33.1 mmol). The reaction was stirred at room temperature for 2 h under an inert atmosphere. The medium was cooled to 0 °C and the precipitate was filtrated and washed with a minimum amount of cold acetone. The 2-thiomethyl-1,3-thiazolium salt was dried under vacuum to afford a white powder in 95% yield (7.5 g). Mp: 146−147 °C. ^{1}H NMR (DMSO-d_6, 300 MHz): δ 1.43 (t, 3H, CH_3, ^3J = 7.3 Hz), 3.01 (s, 3H, CH_3), 4.35 (q, 2H, CH_2, ^3J = 7.3 Hz), 8.14 (d, 1H, HC═, ^3J = 4.0 Hz), 8.45 (d, 1H, HC═, ^3J = 4.0 Hz). ^{13}C NMR (DMSO-d_6, 75 MHz): δ 13.5, 18.6, 48.1, 122.5, 137.1, 174.5. HRMS: calcd for $C_6H_{10}NS_2$ $[C^+]$ 160.025 47, found 160.0254. Anal. Calcd for $C_6H_{10}NIS_2$: C, 25.09; H, 3.51; N, 4.88; S, 22.33. Found: C, 25.25; H, 3.77; N, 4.90; S, 22.42. Sodium methanolate solution (1 M in MeOH, 9.4 mL, 9.4 mmol) was added under an inert atmosphere to a solution of the thiazolium salt (1.8 g, 6.3 mmol) in dry methanol (20 mL). The reaction was stirred at room temperature for 5 h and then extracted with dichloromethane and washed with saturated NaCl solution. The concentrated solution was purified by chromatography on silica gel using CH_2Cl_2/Et_2O (9/1) as eluant to afford thiazoline **2** as a colorless oil in 84% yield (0.68 g). R_f = 0.57 (SiO_2, CH_2Cl_2/Et_2O, 9/1). ^{1}H NMR ($CDCl_3$, 300 MHz): δ 1.31 (t, 3H, CH_3, ^3J = 7.3 Hz), 3.76 (q, 2H, CH_2, ^3J = 7.3 Hz), 6.12 (d, 1H, HC═, ^3J = 5.4 Hz), 6.56 (d, 1H, HC═, ^3J = 5.4 Hz). ^{13}C NMR ($CDCl_3$, 75 MHz): δ = 14.5, 40.2, 101.1, 124.2, 171.7. HRMS: calcd for C_5H_7NONaS $[M + Na]^+$ 152.014 61, found 152.0145.

General Procedure for the Synthesis of the Cyanoethyl Protected Ligands 3 and 4. To a −10 °C cooled solution of thiazoline-2-thione **2** (3.9 mmol, 0.5 g) in dry THF (40 mL) was added a solution of LDA, freshly prepared from *n*-BuLi (5.8 mmol, 3.6 mL, 1.6 M in hexane) and diisopropylamine (5.8 mmol, 0.82 mL) in dry THF (10 mL). After stirring for 30 min at −10 °C, sulfur (5.8 mmol, 0.19 g) or selenium (5.8 mmol, 0.46 g) was added and the solution was stirred for an additional 30 min. To the medium, a solution of LDA (7.8 mmol, 4.9 mL of *n*-BuLi in hexane added to 7.8 mmol, 1.1 mL of diisopropylamine in 10 mL of dry THF) was added. The reaction mixture was stirred at −10 °C for 3 h, and sulfur (7.8 mmol, 0.25 g) or selenium (7.8 mmol, 0.62 g) was added. After 30 min, 3-bromopropionitrile (1.66 mL, 20 mmol) was added and the reaction mixture was stirred overnight. The solvent was evaporated in vacuo, and the residue was extracted with CH_2Cl_2. The concentrated solution was purified by chromatography on silica gel using CH_2Cl_2/Et_2O (95/5) as eluant to afford the protected ligand.

3,3′-[(3-Ethyl-2-oxo-2,3-dihydro-1,3-thiazole-4,5-diyl)bis(thio)]dipropanenitrile 3. Light brown solid in 48% yield (0.56 g). R_f = 0.28 (SiO_2, CH_2Cl_2/Et_2O, 95/5). Mp: 66−67 °C. ^{1}H NMR ($CDCl_3$, 300 MHz): δ 1.30 (t, 3H, CH_3, ^3J = 7.1 Hz), 2.71 (t, 2H, CH_2, ^3J = 7.0 Hz), 2.75 (t, 2H, CH_2, ^3J = 7.0 Hz), 3.06 (t, 2H, CH_2, ^3J = 7.0 Hz), 3.13 (t, 2H, CH_2, ^3J = 7.0 Hz), 4.01 (q, 2H, CH_2, ^3J = 7.1 Hz). ^{13}C NMR ($CDCl_3$, 75 MHz): δ 18.5, 18.6, 31.9, 32.3, 40.9, 116.1, 117.5, 117.7, 131.7, 169.7. HRMS: calcd for $C_{11}H_{14}N_3OS_3$ $[M + H]^+$ 300.0299, found 300.0308. Anal. Calcd for $C_{11}H_{13}N_3OS_3$: C, 44.12; H, 4.38; N, 14.03; S, 32.12. Found: C, 44.04; H, 4.42; N, 13.71; S, 32.67.

3,3′-[(3-Ethyl-2-oxo-2,3-dihydro-1,3-thiazole-4,5-diyl)bis(seleno)]dipropanenitrile 4. Yellow powder in 43% yield (0.66 g). R_f = 0.30 (SiO_2, CH_2Cl_2/Et_2O, 95/5). Mp: 111 °C. ^{1}H NMR (DMSO-d_6, 300 MHz): δ 1.15 (t, 3H, CH_3, ^3J = 7.1 Hz), 2.90−2.96 (m, 4H, CH_2), 3.03−3.12 (m, 4H, CH_2), 3.90 (q, 2H, CH_2, ^3J = 7.1 Hz). ^{13}C NMR (DMSO-d_6, 75 MHz): δ 14.1, 18.4, 18.5, 23.7, 24.8, 41.9, 107.1, 119.4, 119.5, 127.6, 170.9. HRMS: calcd for $C_{11}H_{13}N_3ONaS^{80}Se_2$ $[M + Na]^+$ 417.900 19, found 417.9003. Anal. Calcd for $C_{11}H_{13}N_3OSSe_2$: C, 33.59; H, 3.33; N, 10.68; S, 8.15. Found: C, 33.29; H, 3.42; N, 10.45; S, 8.16.

3,3′-[(3-Ethyl-2-thioxo-2,3-dihydro-1,3-thiazole-4,5-diyl)bis(seleno)]dipropanenitrile 5. A similar procedure as the one described above using 1,3-thiazoline-2-thione **1** (3.45 mmol, 0.5 g) as starting material gave **5** as a yellow solid in 46% yield (0.65 g). R_f = 0.47 (SiO_2, CH_2Cl_2/Et_2O, 19/1). Mp: 134−135 °C. ^{1}H NMR (300 MHz, $CDCl_3$) δ 1.35 (t, 3H, CH_3, ^3J = 7.1 Hz), 2.83−2.89 (m, 4H, CH_2), 3.08−3.17 (m, 4H, CH_2), 4.54 (q, 2H, CH_2, ^3J = 7.1 Hz). ^{13}C NMR (75 MHz, $CDCl_3$) δ 13.3, 19.3, 19.4, 23.6, 25.2, 46.5, 117.7, 117.8, 118.1, 130.8, 188.7. HRMS: calcd for $C_{11}H_{13}N_3S_2{}^{80}Se_2$ $[M^{+\bullet}]$ 410.8881, found 410.8886. Anal. Calcd for $C_{11}H_{13}N_3S_2Se_2$: C, 32.28; H, 3.20; N, 10.26; S, 15.67. Found: C, 32.23; H, 3.20; N, 10.05; S, 15.88.

$[PPh_4][AuS_4(=O)_2]$. To a dry two-necked flask containing thiazoline-2-thione **2** (0.25 g, 0.84 mmol) was added under nitrogen at room temperature 8 mL of 1 M NaOMe in MeOH (8 mmol). The mixture was stirred for 30 min and a solution of $KAuCl_4$ (166 mg, 0.44 mmol) in dry MeOH (12 mL) was slowly added to the medium. The

dx.doi.org/10.1021/ja3065649 | J. Am. Chem. Soc. 2012, 134, 17138−17148

Table 3. Crystallographic Data of Monoanionic Species

compound	$(PPh_4)[AuS_4(=O)_2]$	$(NEt_4)[AuSe_4(=O)_2]$	$(NEt_4)[AuSe_4(=S)_2]$
formula	$C_{34}H_{30}AuN_2O_2PS_6$	$C_{18}H_{30}AuN_3O_2S_2Se_4$	$C_{18}H_{30}AuN_3S_4Se_4$
FW ($g \cdot mol^{-1}$)	918.90	897.38	929.54
crystal system	monoclinic	monoclinic	monoclinic
space group	$C2/c$	$C2/c$	$P2_1/c$
a (Å)	18.3110(6)	17.9569(15)	9.5164(7)
b (Å)	8.0874(3)	10.7960(9)	12.9011(9)
c (Å)	25.3857(8)	14.2220(12)	10.9576(7)
α (deg)	90	90	90
β (deg)	104.610(1)	102.209(4)	96.033(3)
γ (deg)	90	90	90
V (Å^3)	3637.8(2)	2694.8(4)	1337.81(16)
T (K)	150(2)	150(2)	150(2)
Z	4	4	2
D_{calc} (g cm^{-3})	1.678	2.212	2.307
μ (mm^{-1})	4.466	11.037	11.265
total refls	29344	3721	3048
abs corr	multiscan	multiscan	multiscan
uniq refls (R_{int})	4170 (0.0377)	3721	3048
uniq refls ($I > 2\sigma(I)$)	3861	3226	2757
R_1, wR_2	0.0161, 0.0532	0.0426, 0.1246	0.0298, 0.0826
R_1, wR_2 (all data)	0.0219, 0.0782	0.0506, 0.13	0.0356, 0.0852
GOF	1.418	1.137	1.178

Table 4. Crystallographic Data of Neutral Species

compound	$[AuS_4(=O)_2]$	$[AuSe_4(=O)_2]$	$[AuSe_4(=S)_2]$
formula	$C_{10}H_{10}AuN_2O_2S_6$	$C_{10}H_{10}AuN_2O_2S_2Se_4$	$C_{10}H_{10}AuN_2S_4Se_4$
FW ($g \cdot mol^{-1}$)	579.53	767.13	799.25
crystal system	monoclinic	monoclinic	monoclinic
space group	$P2_1/a$	$P2_1/a$	$P2_1/a$
a (Å)	14.135(3)	14.7952(3)	14.5116(5)
b (Å)	4.1370(11)	4.1628(1)	4.0984(3)
c (Å)	13.460(3)	13.4493(3)	14.3554(5)
α (deg)	90	90	90
β (deg)	97.14(3)	95.717(8)	92.613(4)
γ (deg)	90	90	90
V (Å^3)	781.0(3)	824.21(3)	852.89(8)
T (K)	150(2)	150(2)	100(2)
Z	2	2	2
D_{calc} (g cm^{-3})	2.464	3.091	3.112
μ (mm^{-1})	10.222	18.012	17.641
total refls	2024	1857	16837
abs corr	multiscan	multiscan	multiscan
uniq refls (R_{int})	2024	1857	1968 (0.0493)
uniq refls ($I > 2\sigma(I)$)	1439	1374	1774
R_1, wR_2	0.0401, 0.0986	0.0548, 0.1283	0.0206, 0.0393
R_1, wR_2 (all data)	0.0648, 0.121	0.0929, 0.1554	0.0272, 0.0410
GOF	0.961	1.074	1.109

reaction mixture was stirred for 4 h at room temperature, and a solution of PPh_4Cl (0.21 g, 0.55 mmol) was added. After an additional stirring overnight, the precipitate was filtered, washed with MeOH, and recrystallized in CH_3CN to afford the title complex in 30% yield (115 mg) as black crystals. Mp: 206 °C (dec). ^{1}H NMR (CD_3CN, 300 MHz): δ 1.19 (t, 6H, CH_3, ^3J = 7.2 Hz), 3.68 (q, 4H, CH_2, ^3J = 7.2 Hz), 7.64−7.78 (m, 16H, H_{Ar}), 7.89−7.95 (m, 4H, H_{Ar}). HRMS: calcd for $C_{58}H_{50}N_2O_2P_2S_6Au$ $[2C^+,A^-]^+$ 1257.133 75, found 1257.1338. Anal. Calcd for $C_{34}H_{30}N_2O_2PS_6Au$: C, 44.44; H, 3.29; N, 3.05; S, 20.94. Found: C, 44.33; H, 3.24; N, 3.13; S, 21.02.

$[PPh_4][AuSe_4(=O)_2]$. To a two necked flask containing thiazoline-2-thione **2** (0.25 g, 0.64 mmol) was added under nitrogen at room temperature 6 mL of 1 M NaOMe in MeOH (6 mmol). The mixture was stirred for 30 min and a solution of $KAuCl_4$ (132 mg, 0.35 mmol) in 10 mL of dry MeOH was slowly added to the medium. The reaction mixture was stirred for 4 h at room temperature, and a solution of PPh_4Cl (0.19 g, 0.5 mmol) was added. After additional stirring overnight, the precipitate was filtered, washed with MeOH, and recrystallized in CH_3CN to afford the title complex in 27% yield (95 mg) as black crystals. Mp: 213 °C (dec). ^{1}H NMR (CD_3CN, 300 MHz): δ 1.20 (t, 6H, CH_3, ^3J = 7.1 Hz), 3.72 (q, 4H, CH_2, ^3J = 7.1 Hz), 7.64−7.78 (m, 16H, H_{Ar}), 7.89−7.95 (m, 4H, H_{Ar}). HRMS: calcd for $C_{58}H_{50}N_2O_2P_2S_2{}^{80}Se_4Au$ $[2C^+,A^-]^+$ 1448.911 54, found 1448.9139. Anal. Calcd for $C_{34}H_{30}N_2O_2PS_2Se_4Au$: C, 36.90; H, 2.73; N, 2.53; S, 5.79. Found: C, 36.68; H, 2.66; N, 2.66; S, 5.76.

dx.doi.org/10.1021/ja3065649 | J. Am. Chem. Soc. 2012, 134, 17138−17148

$[NEt_4][AuSe_4(=S)_2]$. To a two-necked flask containing 1,3-thiazoline-2-thione **2** (0.25 g, 0.61 mmol) was added 6 mL of 1 M NaOMe in MeOH (6 mmol) under nitrogen at room temperature. The mixture was slowly stirred for 30 min and a solution of $KAuCl_4$ (125 mg, 0.33 mmol) in 10 mL of dry MeOH was slowly added to the medium. The reaction mixture was stirred for 4 h at room temperature, and a solution of NEt_4Br (105 mg, 0.5 mmol) was added. After additional stirring overnight, the precipitate was filtered, washed with MeOH, and recrystallized in CH_3CN to afford the title complex in 50% yield (0.14 g) as black crystals. Mp: 238 °C (dec). ^1H NMR (CD_3CN, 200 MHz): δ 1.21 (m, 12H, CH_3); 1.27 (t, 6H, CH_3, ^3J = 7.1 Hz); 3.16 (q, 8H, CH_2, ^3J = 7.1 Hz); 4.18 (q, 4H, CH_2, ^3J = 7.1 Hz). Anal. Calcd for $C_{18}H_{30}N_3S_4Se_4Au$: C, 23.26; H, 3.25; N, 4.52; S, 13.80. Found: C, 23.30; H, 3.25; N, 4.59; S, 14.15.

Electrocrystallizations. Crystals of $[AuS_4(=O)_2]$, $[AuSe_4(=O)_2]$, or $[AuSe_4(=S)_2]$ were prepared electrochemically using a standard H-shaped cell (12 mL) with Pt electrodes. An acetonitrile solution of $[NEt_4][AuS_4(=O)_2]$ (10 mg), $[PPh_4][AuSe_4(=O)_2]$ (10 mg), or $[PPh_4][AuSe_4(=S)_2]$ (10 mg) was placed in the anodic compartment, and n-Bu_4NPF_6 (100 mg) was placed in both compartments. Black needle crystals of $[AuS_4(=O)_2]$, $[AuSe_4(=O)_2]$, or $[AuSe_4(=S)_2]$ suitable for X-ray diffraction studies were obtained on the anode upon application of a constant current of 0.4 μA for 10 days.

Crystallography. Crystals were picked up with a cryoloop and then frozen at 150 or 100 K under a stream of dry N_2. Data were collected on an APEX II Bruker AXS diffractometer with graphite-monochromated Mo KR radiation (λ = 0.710 73 Å). Structures were solved by direct methods (SIR97)[34] and refined (SHELXL-97)[35] by full-matrix least-squares methods, as implemented in the WinGX software package.[36] Absorption corrections were applied. Hydrogen atoms were introduced at calculated positions (riding model, included in structure factor calculations but not refined). Twin refinement was used for $(NEt_4)[AuSe_4(=O)_2]$, $(NEt_4)[AuSe_4(=S)_2]$, $[AuS_4(=O)_2]$, and $[AuSe_4(=O)_2]$. The two twin domains were determined with the Cell_now program (Bruker AXS), a twin data reduction was done with the SAINT program (Bruker AXS), and a multiscan absorption correction was applied using the Twinabs program (Bruker AXS), generating a HKLF 5 data set constructed from all observations. The elevated GOF value of 1.418 for $(PPh_4)[AuS_4(=O)_2]$ is the consequence of a refinement on an uncut *hkl* data set. The Gof value (1.13) obtained after refinement of a data set cut between 5.5 and 0.77 Å (that remove not well integrated low θ reflections) is closer to the ideal value. Details of the final refinements are given in Table 3 for anionic gold complexes and Table 4 for neutral compounds.

Computational Details. We have used the spin-polarized generalized gradient approximation[37] (σ-GGA) approach to density functional theory[38] (DFT) as implemented in the Vienna Ab Initio Simulation Package (VASP).[39] We used the projector augmented wave[40] method to represent the ionic cores, solving explicitly for the following electrons: 5d and 6s of Au; 3s and 3p of S; 4s and 4p of Se; 2s and 2p of O, N, and C; and 1s of H. Electronic wave functions were represented with a plane wave basis truncated at 400 eV. A careful convergence test for Brillouin zone integrations was necessary. Accurate energy differences between various (e.g., antiferromagnetic vs metallic) electronic solutions were obtained using Γ-centered 4 × 8 × 4 *k*-point grids for the simulation cell with four molecules in it, which results from the crystalline cell (two molecules) and an antiferromagnetic ordering along *b*.

Resistivity Measurements. The resistivity has been measured along the long axis of the needles (*b* crystallographic axis). Gold pads were evaporated on the surface of the crystals in order to improve the quality of the contacts. Then a standard four-points technique was used with a low frequency lock-in detection (I_{ac} = 0.1−1 μA) for measured resistances below 50 kΩ and dc measurement for higher resistances (I_{dc} = 0.1−0.01 μA). Hydrostatic pressures were applied at room temperature in a NiCrAl clamp cell using Daphne 7373 silicone oil as the pressure transmitting medium. The pressure was determined, at room temperature, using a manganin resistance gauge located in the pressure cell close to the sample. The pressures indicated here are room temperature values, and the loss of pressure occurring during cooling is estimated to 2 kbar. Low temperatures have been provided by cryocooler equipment down to 25 K except for experiments under pressure on $[AuSe_4(=S)_2]$, which were performed in a variable-temperature insert in an helium cryostat down to 1.5 K.

■ ASSOCIATED CONTENT

Ⓢ Supporting Information

X-ray crystallographic files in CIF format and cyclic voltamogram of $[AuSe_4(=S)_2]$. This material is available free of charge via the Internet at http://pubs.acs.org.

■ AUTHOR INFORMATION

Corresponding Author

dominique.lorcy@univ-rennes1.fr; marc.fourmigue@univ-rennes1.fr; canadell@icmab.es

Notes

The authors declare no competing financial interest.

■ ACKNOWLEDGMENTS

Financial support from University Rennes 1 for a Ph.D. grant (to G.Y.) is gratefully acknowledged. We thank the CDIFX (Rennes, France) for access to X-ray data collection facilities. This work was also supported by MINECO-Spain (Projects FIS2009-12721-C04-03, MAT2010-18113, MAT2010-10093 and CSD2007-00041).

■ REFERENCES

(1) Kato, R. *Chem. Rev.* **2004**, *104*, 5319−5346.

(2) Kobayashi, A.; Fujiwara, E.; Kobayashi, H. *Chem. Rev.* **2004**, *104*, 5243−5264.

(3) Sasa, M.; Fujiwara, E.; Kobayashi, A.; Ishibashi, S.; Terakura, K.; Okano, Y.; Fujiwara, H.; Kobayashi, H. *J. Mater. Chem.* **2005**, *15*, 155−163.

(4) Neutral gold complexes with a TTF dithiolene backbone are highly insoluble, such as $[Au(tmdt)_2]$, a magnetic metal exhibiting an antiferromagnetic transition at 110 K, or a semiconducting $[Au(ptdt)_2]$: (a) Suzuki, W.; Fujiwara, E.; Kobayashi, A.; Fujishiro, Y.; Nishibori, E.; Takata, M.; Sakata, M.; Fujiwara, H.; Kobayashi, H. *J. Am. Chem. Soc.* **2003**, *125*, 1486−1487. (b) Zhou, B.; Shimamura, M.; Fujiwara, E.; Kobayashi, A.; Higashi, T.; Nishibori, E.; Sakata, M.; Cui, H.; Takahashi, K.; Kobayashi, H. *J. Am. Chem. Soc.* **2006**, *128*, 3872−3873. (c) Zhou, B.; Yajima, H.; Idobata, Y.; Kobayashi, A.; Kobayashi, T.; Nishibori, E.; Sawa, H.; Kobayashi, H. *Chem. Lett.* **2012**, *41*, 154−156.

(5) Schiødt, N. C.; Bjørnholm, T.; Bechgaard, K.; Neumeier, J. J.; Allgeier, C.; Jacobsen, C. S.; Thorup, N. *Phys. Rev. B* **1996**, *53*, 1773−1778.

(6) Belo, D.; Alves, H.; Lopes, E. B.; Duarte, M. T.; Gama, V.; Henriques, R. T.; Almeida, M.; Pérez-Benítez, A.; Rovira, C.; Veciana, J. *Chem.—Eur. J.* **2001**, *7*, 511−519.

(7) Dautel, O. J.; Fourmigué, M.; Canadell, E.; Auban-Senzier, P. *Adv. Funct. Mater.* **2002**, *12*, 693−698.

(8) (a) Eid, S.; Fourmigué, M.; Roisnel, T.; Lorcy, D. *Inorg. Chem.* **2007**, *46*, 10647−10654. (b) Eid, S.; Guerro, M.; Lorcy, D. *Tetrahedron Lett.* **2006**, *47*, 8333−8336. (c) Eid, S.; Roisnel, T.; Lorcy, D. *J. Organomet. Chem.* **2008**, *693*, 2755−2760.

(9) Tenn, N.; Bellec, N.; Jeannin, O.; Piekara-Sady, L.; Auban-Senzier, P.; Iniguez, J.; Canadell, E.; Lorcy, D. *J. Am. Chem. Soc.* **2009**, *131*, 16961−16967.

(10) Very few X-ray crystal structure of TTF derivatives performed under pressure are available: (a) Schultz, A. J.; Wang, H. H.; Williams, J. M; Filhol, A. *J. Am. Chem. Soc.* **1986**, *108*, 7853−7855. (b) Molchanov, V. N.; Shibaeva, R. P.; Kachinskii, V. N.; Yagubskii, E. B.; Simonov, V. I.; Vainstein, B. K. *Dokl. Akad. Nauk. SSSR* **1986**, *286*, 637−640. (c) Guionneau, P.; Gaultier, J.; Rahal, M.; Bravic, G.;

Mellado, J. M.; Chasseau, D.; Ducasse, L.; Kurmoo, M.; Day, P. *J. Mater. Chem.* **1995**, *5*, 1639−1645. (d) Rahal, M.; Chasseau, D.; Gaultier, J.; Ducasse, L.; Kurmoo, M.; Day, P. *Acta Crystallogr. B* **1997**, *53*, 159−167. (e) Filhol, A.; Bravic, G.; Gaultier, J.; Chasseau, D.; Vettier, C. *Acta Crystallogr. B* **1981**, *37*, 1225−1235. (f) Gallois, B.; Gaultier, J.; Hauw, C.; Lamcharfi, T.-D.; Filhol, A. *Acta Crystallogr. B* **1986**, *42*, 564−575. (g) Okano, Y.; Zhou, B.; Tanaka, H.; Adachi, T.; Oshihi, Y.; Takata, M.; Aoyagi, S.; Nishibori, E.; Sakata, M.; Kobayashi, A.; Kobayashi, H. *J. Am. Chem. Soc.* **2009**, *131*, 7169−7174.

(11) Jérome, D. *Chem. Rev.* **2004**, *104*, 5565−5591.

(12) (a) Kagoshima, S.; Kondo, R. *Chem. Rev.* **2004**, *104*, 5593−5608. (b) Murata, K.; Kagoshima, S.; Yasuzuka, S.; Yoshino, H.; Kondo, R. *J. Phys. Soc. Jpn.* **2006**, *75*, 051015/1−051015/15.

(13) (a) Coulon, C.; Parkin, S. S. P.; Laversanne, R. *Phys. Rev. B* **1985**, *31*, 3583−3587. (b) Nad, F.; Monceau, P. *J. Phys. Soc. Jpn.* **2006**, *75*, 051005/1−051005/12. (c) Zamborszky, F.; Yu, W.; Raas, W.; Brown, S. E.; Alavi, B.; Merlic, C. A.; Baur, A. *Phys. Rev. B* **2002**, *66*, 081103/1−081103/4.

(14) Kohler, B.; Rose, E.; Dumm, M.; Untereiner, G.; Dressel, M. *Phys. Rev. B* **2011**, *84*, 035124/1−035124/13.

(15) Ilakovac, V.; Ravy, S.; Boubekeur, K.; Lenoir, C.; Batail, P.; Pouget, J. P. *Phys. Rev. B* **1997**, *56*, 13878−13887.

(16) Note that the location of the anion within the soft cavities formed by methyl or methylene groups in these salts plays a role that goes beyond a simple chemical presure effect. See: Pouget, J.-P. *Crystals* **2012**, *2*, 466−520.

(17) (a) Geiser, U.; Schults, A. J.; Wang, H. H.; Watkins, D. M.; Stupka, D. L.; Williams, J. M.; Schirber, J. E.; Overmyer, D. L.; Jung, D.; Novoa, J. J.; Whangbo, M.-H. *Physica C* **1991**, *174*, 475−486. (b) Yasin, S.; Dumm, M.; Salameh, B.; Batail, P.; Mézière, C.; Dressel, M. *Eur. Phys. J. B* **2011**, *79*, 383−390. (c) Dumm, M.; Faltermeier, D.; Drichko, N.; Dressel, M.; Meziere, C.; Batail, P. *Phys. Rev. B* **2009**, *79*, 195106/1−195106/11.

(18) (a) Fourmigué, M.; Reinheimer, E. W.; Dunbar, K. R.; Auban-Senzier, P.; Pasquier, C.; Coulon, C. *Dalton Trans* **2008**, 4652−4658. (b) Foury-Leylekian, P.; Auban-Senzier, P.; Coulon, C.; Jeannin, O.; Fourmigué, M.; Pasquier, C.; Pouget, J.-P. *Phys. Rev. B* **2011**, *84*, 195134. (c) Reinheimer, E. W.; Assaf, A.; Jeannin, O.; Benallouche, A.; Nguyen, P.-T.; Coulon, C.; Fourmigué, M. *Phys. Status Solidi* **2012**, *B249*, 943−946.

(19) (a) Zorina, L.; Simonov, S.; Meziere, C.; Canadell, E.; Suh, S.; Brown, S. E.; Foury-Leylekian, P.; Fertey, P.; Pouget, J.-P.; Batail, P. *J. Mater. Chem.* **2009**, *19*, 6980−6994. (b) Heuzé, K.; Fourmigué, M.; Batail, P.; Coulon, C.; Clérac, R.; Canadell, E.; Auban-Senzier, P.; Ravy, S.; Jérome, D. *Adv. Mater.* **2003**, *15*, 1251−1253.

(20) (a) Coldea, A. I.; Bangura, A. F.; Singleton, J.; Ardavan, A.; Akutsu-Sato, A.; Akutsu, H.; Turner, S. S.; Day, P. *Phys. Rev. B* **2004**, *69*, 085112. (b) Bangura, A. F.; Coldea, A. I.; Singleton, J.; Ardavan, A.; Akutsu-Sato, A.; Akutsu, H.; Turner, S. S.; Day, P.; Yamamoto, T.; Yakushi, K. *Phys. Rev. B* **2005**, *72*, 014543.

(21) Yoneyama, N.; Sasaki, T.; Kobayashi, N. *J. Phys. Soc. Jpn.* **2004**, *73*, 1434−1437.

(22) Sinzger, K.; Hunig, S.; Jopp, M.; Bauer, D.; Bietsch, W.; von Schutz, J. U.; Wolf, H. C.; Kremer, R. K.; Metzenthin, T.; Bau, R.; Khan, S. I.; Lindbaum, A.; Lengauer, C. L.; Tillmanns, E. *J. Am. Chem. Soc.* **1993**, *115*, 7696−7705.

(23) (a) Matsunaga, N.; Ayari, A.; Monceau, P.; Ishikawa, A.; Nomura, K.; Watanabe, M.; Yamada, J.; Nakatsuji, S. *Phys. Rev. B* **2002**, *66*, 024425. (b) Cooper, J. R.; Lukatela, J.; Miljak, M.; Fabre, J.-M.; Giral, L.; Aharon-Shalom, E. *Solid State Commun.* **1978**, *25*, 949−954. (c) Dalal, N. S.; Haley, L. V.; Northcott, D. J.; Park, J. M.; Reddoch, A. H.; Ripmeester, J. A.; Williams, D. F. *J. Chem. Phys.* **1980**, *73*, 2515−2517.

(24) (a) Kawamoto, A.; Miyagawa, K.; Kanoda, K. *Phys. Rev. B* **1997**, *55*, 14140. (b) Miyagawa, K.; Kawamoto, A.; Kanoda, K. *Phys. Rev. Lett.* **2002**, *89*, 017003. (c) Kini, A. M.; Carlson, K. D.; Wang, H. H.; Schlueter, J. A.; Dudek, J. D.; Sirchio, S. A.; Geiser, U.; Lykke, K. R.; Williams, J. M. *Physica C* **1996**, *264*, 81−94.

(25) (a) Suzuki, W.; Fujiwara, E.; Kobayashi, A.; Fujishiro, Y.; Nishibori, E.; Takata, M.; Sakata, M.; Fujiwara, H.; Kobayashi, H. *J. Am. Chem. Soc.* **2003**, *125*, 1486. (b) Zhou, B.; Shimamura, M.; Fujiwara, E.; Kobayashi, A.; Higashi, T.; Nishibori, E.; Sakata, M.; Cui, H.; Takahashi, K.; Kobayashi, H. *J. Am. Chem. Soc.* **2006**, *128*, 3872. (c) Hara, Y.; Miyagawa, K.; Kanoda, K.; Shimamura, M.; Zhou, B.; Kobayashi, A.; Kobayashi, H. *J. Phys. Soc. Jpn.* **2008**, *77*, 053706.

(26) Okano, Y.; Zhou, B.; Tanaka, H.; Adachi, T.; Ohishi, Y.; Takata, M.; Aoyagi, S.; Nishibori, E.; Sakata, M.; Kobayashi, A.; Kobayashi, H. *J. Am. Chem. Soc.* **2009**, *131*, 7169−7174.

(27) *Stable Radicals*; Hicks, R. G., Ed.; John Wiley & Sons: Chichester (UK), 2010.

(28) (a) Leitch, A. A.; Reed, R. W.; Robertson, C. M.; Britten, J. F.; Yu, X.; Secco, R. A.; Oakley, R. T. *J. Am. Chem. Soc.* **2007**, *129*, 7903−7914. (b) Yu, X.; Mailman, A.; Dube, P. A.; Assoud, A.; Oakley, R. T. *Chem. Commun.* **2011**, *47*, 4655−4657. (c) Yu, X.; Mailman, A.; Lekin, K.; Assoud, A.; Robertson, C. M.; Noll, B. C.; Campana, C. F.; Howard, J. A. K.; Dube, P. A.; Oakley, R. T. *J. Am. Chem. Soc.* **2012**, *134*, 2264−2275. (d) Yu, X.; Mailman, A.; Lekin, K.; Assoud, A.; Dube, P. A.; Oakley, R. T. *Cryst. Growth Des.* **2012**, *12*, 2485−2494.

(29) (a) Leitch, A. A.; Lekin, K.; Winter, S. M.; Downie, L. E.; Tsuruda, H.; Tse, J. S.; Mito, M.; Desgreniers, S.; Dube, P. A.; Zhang, S.; Liu, Q.; Jin, C.; Ohishi, Y.; Oakley, R. T. *J. Am. Chem. Soc.* **2011**, *133*, 6051. (b) Mailman, A.; Winter, S. M.; Yu, X.; Robertson, C. M.; Yong, W.; Tse, J. S.; Secco, R. A.; Liu, Z.; Dube, P. A.; Howard, J. A. K.; Oakley, R. T. *J. Am. Chem. Soc.* **2012**, *134*, 9886−9889.

(30) Schultz, A. J.; Wang, H. H.; Soderholm, L. C.; Sifter, T. L.; Williams, J. M.; Bechgaard, K.; Whangbo, M.-H. *Inorg. Chem.* **1987**, *26*, 3757−3761.

(31) Geiser, U.; Schultz, A. J.; Wang, H. H.; Beno, M. A.; Williams, J. M. *Acta Crystallogr., Sect C* **1988**, *44*, 259−262.

(32) Kokatam, S.; Ray, K.; Pap, J.; Bill, E.; Geiger, W. E.; Le Suer, R. J.; Rieger, P. H.; Weyhermüller, T.; Neese, F.; Wieghardt, K. *Inorg. Chem.* **2007**, *46*, 1100−1111.

(33) Jérome, D. *Science* **1991**, *252*, 1509−1514.

(34) Altomare, A.; Cascarano, G.; Giacovazzo, C.; Guagliardi, A.; Burla, M. C.; Polidori, G.; Camalli, M. *J. Appl. Crystallogr.* **1994**, *27*, 435−436.

(35) Sheldrick, G. M. *SHELX97—Programs for Crystal Structure Analysis, Release 97−2*; 1998.

(36) Farrugia, L. J. *J. Appl. Crystallogr.* **1999**, *32*, 837−838.

(37) Perdew, J. P.; Burke, K.; Ernzerhof, M. *Phys. Rev. Lett.* **1996**, *77*, 3865−3868.

(38) (a) Hohenberg, P; Kohn, W. *Phys. Rev.* **1964**, *136*, B864−B871. (b) Kohn, W.; Sham, L. J. *Phys. Rev.* **1965**, *140*, A1133−A1138.

(39) Kresse, G.; Furthmuller, J. *Phys. Rev. B* **1996**, *54*, 11169−11186.

(40) (a) Blochl, P. E. *Phys. Rev B* **1994**, *50*, 17953−17979. (b) Kresse, G.; Joubert, D. *Phys. Rev. B* **1999**, *59*, 1758−1775.